Materials Chemistry and Physics 311 (2024) 128548

Contents lists available at ScienceDirect

Materials Chemistry and Physics

journal homepage: www.elsevier.com/locate/matchemphys

Kinetic study of Cu_2S–FeS mixtures in an oxidative environment by thermogravimetric and thermodynamic analysis

M. Vázquez Vázquez [a,*], M.J. Díaz Blanco [b,c], R.A. Parra Figueroa [d], E.R. Balladares Varela [d], O. Jerez Riveros [e], M. Cuevas Cerda [d], I. Moreno-Ventas Bravo [a,f]

[a] Faculty of Experimental Science, University of Huelva, 21007, Huelva, Spain
[b] Higher Technical School of Engineering, University of Huelva, 21007, Huelva, Spain
[c] Centre for Research in Product Technology and Chemical Processes (Pro2TecS), University of Huelva, 21007, Huelva, Spain
[d] Metallurgical Engineering Department, University of Concepción, 4070386, Concepción, Chile
[e] Institute of Applied Economic Geology, University of Concepción, 4070386, Concepción, Chile
[f] Center for Research in Sustainable Chemistry (CIQSO), University of Huelva, 21007, Huelva, Spain

HIGHLIGHTS

- Thermal oxidation evolution of Cu2S–FeS mixtures has been studied by thermogravimetry.
- Among the methods studied for kinetic analysis, KAS method appears the most suitable.
- TGA curve of Cu2S–FeS has been reproduced by computational thermodynamic calculations.
- The chemical reactions involved in the oxidation of Cu2S–FeS have been determined.

GRAPHICAL ABSTRACT

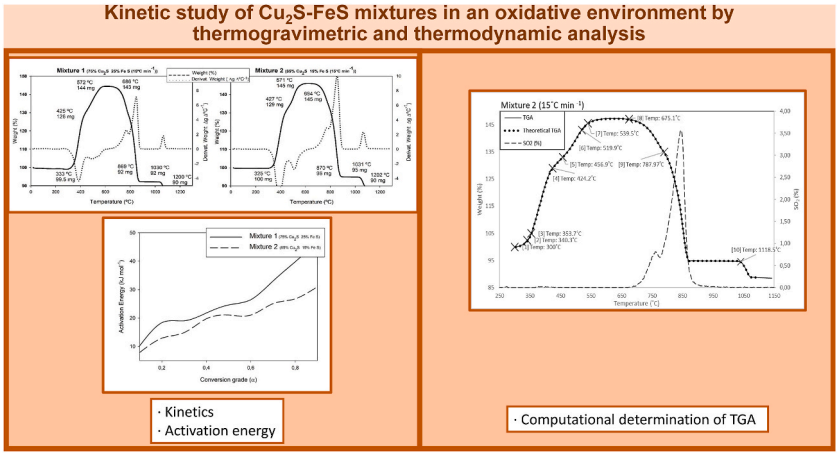

ARTICLE INFO

Keywords:
Copper
Thermodynamic
FactSage
Thermogravimetric analysis
Kinetic

ABSTRACT

Two samples of Cu_2S–FeS mixtures were prepared in order to study the thermal oxidation evolution of the raw materials used during the first and second sub-stages of slag blowing in a converter furnace. To determine the thermal evolution in an oxidative environment, thermogravimetric analysis (TGA) was performed on both samples at four linear heating ramps (5, 10, 15 and 20 °C min^{-1}), obtaining similar curves in both cases. Of the methods studied, Friedman, Coats-Redfern, Flynn-Wall-Ozawa and Kissinger-Akahira-Sunose, the latter was found to be the most suitable to represent the oxidative evolution of Cu_2S–FeS mixtures. The kinetic parameters calculated using Kissinger-Akahira-Sunose method are highly dependent on the degree of conversion. The results obtained for the activation energy ranging between 10 and 20 Kj mol^{-1} for conversion rates of 0.2, and between

* Corresponding author.
E-mail address: dblanco@uhu.es (M.J. Díaz Blanco).

https://doi.org/10.1016/j.matchemphys.2023.128548
Received 25 May 2023; Received in revised form 21 August 2023; Accepted 9 October 2023
Available online 10 October 2023

30 and 50 Kj mol^{-1} for conversion rates of 0.9. In addition, a thermodynamic computational model was developed to determine the reactions taking place during the oxidation of the Cu_2S–FeS mixtures.

1. Introduction

Extractive metallurgy of copper involves two industrial processes: pyrometallurgy and hydrometallurgy. Copper from low-grade oxidized ores is extracted by hydrometallurgy in three main stages, leaching, solvent and electrowinning, while pyrometallurgy is the main process to obtain copper from copper sulfide ores [1].

The pyrometallurgy of copper causes the oxidative melting of the starting material to occur across several stages. The first is flash smelting from a blend of copper concentrate, flux and recycled material [2].

Flash smelting produces two immiscible liquids, matte and slag. The slag is mainly composed of Magnetite (Fe_3O_4) and Fayalite (Fe_2SiO_4) while the matte consists of a mixture of iron and copper sulfur phases (FeS and Cu_2S). In general, the flash smelting process follows the reactions (Eqs. (1)–(3)) [1,3]. The main product of flash smelting is matte, with a grade of 62–65 %.

$$CuFeS_2 + 3.25\ O_2 = Cu_2S + 0.5\ FeS + 1.5\ FeO + 2.5\ SO_2 \quad \text{Eq. 1}$$

$$3\ FeS + 5\ O_2 = Fe_3O_4 + 3\ SO_2 \quad \text{Eq. 2}$$

$$2\ FeO + SiO_2 = Fe_2SiO_4 \quad \text{Eq. 3}$$

The molten matte is usually processed in a converter furnace, the most common of which is the Peirce-Smith version [4,5]. This furnace processes in batches, so the matte from flash smelting is processed in two stages, the first being slag blowing.

In slag blowing, the matte is processed from flash smelting and sometimes also from copper recovery in slag. The recovered matte usually has a higher concentration of copper than the matte from flash smelting. After charging with matte, flux (usually SiO_2) is added to the converter furnace. Oxygen-enriched air is blown into this melt through the tuyeres at the bottom of the furnace [1]. The matte oxidation process generally follows reactions 2 and 4:

$$3\ FeS + 1.5\ O_2 = FeO + SO_2 \quad \text{Eq. 4}$$

During slag blowing, the matte converter furnace is usually recharged in order to process a larger amount of material. Recharging takes place immediately after the first skimming of the slag produced. Therefore, the slag-blowing stage can be divided into two sub-stages. Sub-stage 1 starts with the processing of the matte with approximately 62–65%Cu, and ends with the first skimming and matte recharged, while sub-stage 2 starts with the second processing of the matte with approximately 70–75%Cu, and ends with the second skimming and the copper-rich molten phase as white metal (Approx. 80%Cu).

The second stage of the converter process is copper blowing, in which the white metal is oxidized to remove the sulfur contained in the white metal in the form of SO_2 in the gas phase. The general reactions that follow this process are Eqs. (5) and (6).

$$Cu_2S + 1.5\ O_2 = Cu_2O + SO_2 \quad \text{EQ 5}$$

$$Cu_2S + 2Cu_2O = 6Cu + SO_2 \quad \text{EQ 6}$$

The aim of this work was to study the kinetics of the slag-blowing stage of the conversion process. For this purpose, two starting materials were used: Mixture_1, similar to a matte with 65%Cu; Mixture_2, similar to a matte with 73%Cu, resembling the first and second sub-stages of the slag blowing of the conversion process.

These industrial processes require rigorous control of operational parameters, such as the temperatures applied, the air enrichment used or the number of times required for each oxidation process, among others [3]. The correct adjustment of these and other parameters is crucial for minimizing costs in the extraction of copper by pyrometallurgy. This study applied the relevant adjustments to improve the conversion process during the slag-blowing stage by studying the kinetic evolution of two mixtures composed of different proportions of Cu_2S and FeS. The Friedman, Coats, Kissinger and Flynn kinetic methods were evaluated and the most appropriate one used in this study.

As an innovation, we studied the chemical reactions in the oxidation process of the Cu_2S–FeS mixture by applying a computational thermodynamics model developed for this study. This model provides a computational calculation of all reactions and their working temperatures. For this purpose, we made a computational reproduction of the experimental results of the real mass loss/gain curve obtained by thermogravimetry (TGA).

2. Materials and methods

2.1. Starting materials

The raw material used in this study was Cu_2S and FeS obtained from Fisher Scientific. Cu_2S has a formula weight of 159.14 g mol^{-1}, a density of 5.6 g ml^{-1} and a purity of 99.5 %; FeS has a formula weight of 87.91 g mol^{-1}, a density of 4.7 g ml^{-1} and a purity of 99.98 %. This study acquired Cu_2S and FeS with a mesh powder of less than 200 μm.

Two mixtures were prepared, Mixture_1 and Mixture_2. To produce these mixtures, Cu_2S and FeS were mixed proportionally to achieve compositions similar to the first and second sub-stages of the slag-blowing conversion process. Each amount of Cu_2S and FeS was weighed on an analytical electrobalance. To ensure mixture homogenization, a Fritsch Pulverisette ball mill was used, running for 5 min at 450 r.p.m.

Both mixtures were analyzed using Rigaku X-Ray fluorescence spectrometer (FRX) model ZSX primus II. In both cases, the impurities in the mixtures amounted to less than 0.5 % in each sample.

Mixture_1 had a matte grade of 65.6 %, similar to the matte to be processed in the converter furnace during the first sub-stage of slag blowing. The composition of Mixture_1 is shown in Table 1.

Mixture_2 contained a matte grade of 72.8 %, similar to the matte to be processed in the converter furnace during the second stage of slag blowing. The composition of Mixture 2 is shown in Table 2.

2.2. DOAS

The gasses produced during the TGA test were examined using a differential optical absorption spectroscopy analyzer (DOAS) (Unisearch Associates Inc.). This equipment takes the SO_2 absorption signals and compares them to the equipment's own patterns to determine the concentration of SO_2 produced per unit time. The concentration range that the analyzer is able to analyze is wide, as it uses 4 simultaneous analysis channels ranging from high SO_2 concentrations to the ppm scale [6, 7].

2.3. TGA

Thermogravimetric analysis (TGA) is a suitable instrument for

Table 1
Composition of Mixture_1 (65 wt% Cu) obtained by FRX.

Element	Mass	Detection limit	Element	Mass	Detection limit
Cu	65.60	0.01	Si	0.032	0.004
S	19.74	0.02	Sn	0.031	0.009
Fe	14.50	0.01	Ni	0.025	0.006

Table 2
Composition of Mixture_2 (73 wt% Cu) obtained by FRX.

Element	Mass	Detection limit	Element	Mass	Detection limit
Cu	72.79	0.01	Al	0.050	0.005
S	18.49	0.02	Sn	0.040	0.009
Fe	8.55	0.01	Si	0.020	0.004

determining kinetic behavior in the oxidation process of Cu_2S–FeS mixtures.

This equipment provides accurate information about the weight loss/gain of the sample as a function of temperature. A thermogravimetric analyzer (Simultaneous Thermal Analysis 449 F3 Jupiter, NETZSCH) was used to verify the thermochemical response of the mixtures studied. The TGA experiments were carried out by heating samples of approximately 50 mg from 25 °C to 1300°C at four heating rates of 5, 10, 15 and 20°C min^{-1}, respectively, under an oxygen flow rate of 20 cm^3 min^{-1}. Each test condition was carried out in triplicate in order to verify the representativeness of the results.

2.4. Kinetic methods

Thermogravimetry and differential thermogravimetry (DTGA) techniques were applied to calculate kinetic parameters in oxidation reactions [8–10]. The kinetic methods used in this work are based in the Arrenius equation (Eq. 7). In accordance with the ICTAC (International Confederation of Thermal Analysis and Calorimetry) Kinetics Committee [11], different isoconversional methods were used to evaluate the evolution of the kinetic parameters of the reactions in the oxidative degradation of the mixtures. The kinetic parameters calculated were activation energy (Ea), pre-exponential factor (A) and reaction order (n).

$$\frac{d(\alpha)}{dt} = k(T) f(\alpha) \qquad \text{Eq. 7}$$

Where: dα/dt is the reaction rate (min^{-1}), α is the fractional conversion, *k(T)* is the rate constant and *f(α)* is a function of reaction degree.

Substituting the Arrhenius equation in Eq. (7), Eq. (8) can be obtained.

$$\frac{d(\alpha)}{dt} = A\ e^{\left(-\frac{Ea}{RT}\right)}\ f(\alpha) \qquad \text{Eq. 8}$$

Where: *A* is the pre-exponential factor (min^{-1}), Ea is the apparent activation energy (J mol^{-1}), T is the temperature (K) and R is the ideal gas constant (8.314 J mol^{-1} K^{-1}) [12].

After rearranging and integrating the above equation, Eq. (9) can be obtained.

$$g(\alpha) = \int_0^{\alpha} \frac{d(\alpha)}{f(\alpha)} = \frac{A}{\beta} \int_{T0}^{T} e^{\left(-\frac{Ea}{RT}\right)} dT \qquad \text{Eq. 9}$$

Where g(α) is the integral form of f(α), β is the heating rate (K min^{-1}), T_0 is the initial temperature (K) and T is the final temperature (K) of the non-isothermal experiment.

The function g(α) is a general parameter that will depend on each reaction, but may also involve several reactions. Thus, multiple reactions that can take place at about the same temperature and, with its specific conversion rate, are part of a general function that can involve the conversion rate of the total system. To facilitate the calculations, different approximations to give g(α) [13–16] were developed. Table 3 presents the approximations analyzed in this study.

Netzsch Kinetics Neo software (v2.1.2.1) was used to determine Ea using the methods described above.

Table 3
Mathematical expression[a] to calculate kinetic degradation.

Method		Reference
Friedman	$ln\left(\frac{d\alpha}{dt}\right) = ln\left(A f(\alpha)\right) - \frac{Ea}{RT}$ (Eq. 10)	[13]
Coats - Redfern	$ln\frac{g(\alpha)}{T^2} = ln\frac{A R}{\beta E}\left(1 - \frac{2 R T}{Ea}\right) - \frac{Ea}{RT}$ (Eq. 11)	[14]
	- First order $g(x) = -ln(1-\alpha)^2$	[17]
	- Second order $g(x) = (1-\alpha)^{-1} - 1$	
Kissinger -Akahira -Sunose (KAS)	$ln\left(\frac{\beta}{T^2}\right) = ln\left(\frac{A R}{g(\alpha)\ Ea}\right) - \frac{Ea}{RT}$ (Eq. 12)	[15]
Flynn - Wall -Ozawa (FWO)	$log(\beta) = log\left[\frac{A\ Ea}{g(\alpha)\ R}\right] - 2.315 - \frac{0.457\ Ea}{RT}$ (Eq. 13)	[16,18]

[a] Different selected functions for f(α) and g(α) depending on the selected model and reaction order.

2.5. Reaction determination by thermodynamic modelling

The reactions that occur during the oxidation of mixtures composed of different proportions of Cu_2S–FeS were determined by thermodynamic calculations. The Equilib module of the FactSage program was used for this purpose [19–22]. This software uses the Gibbs energy minimization method to calculate the association of equilibrium phases and their composition.

The main objective of the modeling was to fit the thermodynamic calculations results to reproduce the empirical curve of the TGA test. Short increasing temperature ranges were applied for the calculations, and the reactions that occurred for the oxidation of Cu_2S-Fes mixtures in these temperature ranges were determined in each case.

To develop the thermodynamic model, it was necessary to know all the starting conditions of the system studied. The model parameters used for each calculation step were the composition of the starting material, the composition of the working gas and the initial temperature of the thermal range. The main parameters that were adjusted during each calculation step were the mass inside the crucible, the working gas efficiency during oxidation, and the temperature variation. In each calculation step, the initial composition was assumed to be the final composition of the immediately preceding system. Working gas efficiency during oxidation was used to reproduce the temperature-mass pairs reported in the results of the empirical TGA test. The temperature variation used in each calculation step was 0.1°C, for which the chemical equilibrium of the oxidative process of the Cu_2S–FeS mixtures was calculated. The total temperature range modeled expanded from 25°C to 1300°C. The last system studied was determined by the no-mass variation based on the empirical TGA test.

3. Results and discussion

3.1. TGA comparative analysis

Fig. 1 shows the thermograms corresponding to the mass evolution (TGA) and its derivative curve (DTG), with respect to the temperature corresponding to their oxidative reactions at 15°C min^{-1}, for the two studied samples.

The curves in Fig. 1 for the studied mixtures show similar behavior to those described by Schwab and Philinis [23] for pyrite oxidation, and by Prasad and Pandey [24] for iron sulfide oxidation. In both cases, the samples initially gained weight, leveled off and subsequently decreased in weight.

Fig. 1 shows the similarity in the evolution of the studied mixtures. Nevertheless, small differences in the DTG peaks of samples 1 and 2 can be observed.

In this figure, the TGA curve for both samples indicates an absence of either weight loss or weight gain (absence of chemical reaction) up to 325-333°C, after which different phases can be observed for both

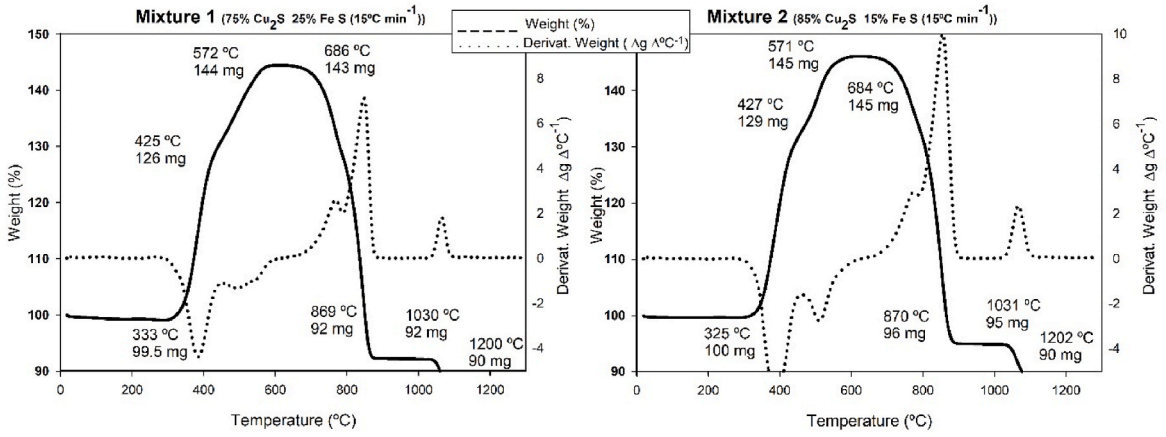

Fig. 1. TGA and DTG corresponding to the oxidative reactions in the Cu_2S–FeS mixtures at 15 °C min^{-1}.

samples and according to temperature. Six phases could be identified that were produced during the thermal increase in the TGA experiment for the two studied samples.

TGA Stage I, corresponding to 325–425°C. A weight increase in this temperature range in both TGA curves was observed. Based on data collected by Coombs and Munir [25] sulfate formation in iron and copper is likely to occur in the range of 300-500 °C. It is generally accepted that ferrous sulfate ($FeSO_4$) is formed initially (at 200°C and above), subsequently oxidizing into ferric sulfate. Oxidation to ferric sulfate at temperatures similar to 327°C has been observed by Kennedy and Sturman [26].

In this stage, sulfate formation of the metal sulfides takes place. The equations proposed by Dunn and Muzeda [27], Coombs and Munir [24] and Asaki and Kondo [28] for the reactions occurring at the temperature corresponding to Stage 1 are Eq.14-20.

$$2Cu_2S + \frac{9}{2}\,O_2 = Cu_2O + 2\,CuSO_4 \quad \text{(Eq .14)}$$

$$Cu_2S + 2O_2 = Cu_2SO_4 \quad \text{(Eq .15)}$$

$$Fe\,S + \frac{2}{3}x\,O_2 \rightarrow Fe_{1-x}\,S + \frac{x}{3}\,Fe_3\,O_4 \quad \text{(Eq. 16)}$$

$$Fe\,S + \frac{3}{4}x\,O_2 \rightarrow Fe_{1-x}\,S + \frac{x}{2}\,Fe_2\,O_3 \quad \text{(Eq. 17)}$$

$$2Fe_3\,O_4 + \frac{1}{2}\,O_2 \rightarrow 3\,Fe_2\,O_3 \quad \text{(Eq. 18)}$$

$$2\,Fe\,S + 5\,O_2 + SO_2 \rightarrow Fe_2\,(SO_4)_3 \quad \text{(Eq. 19)}$$

$$2\,Fe_2\,(SO_4)_3 \rightarrow 2\,Fe_2O_3 + 6\,SO_2 + 3\,O_2 \quad \text{(Eq. 20)}$$

The crucible weight increase is a consequence of the above reactions due to the oxygen uptake implied. A weight increase in the studied samples of 26 % for Mixture_1 (65 wt% Cu) and 29 % for Mixture_2 (73 wt% Cu) was observed.

These results match those reported by Schwab and Philinis [23] for pyrite. These authors indicated that the maximum weight loss (18.2 % at 500°C) corresponds to the formation of ferrous oxide. As the temperature increased, the observed weight loss was less. These changes correspond to increasing sulfate formation at low temperatures. Thus, the main reactions can be represented by the following equations:

$$2\,Cu\,Fe\,S_2 + 7.5\,O_2 \rightarrow 2\;Cu\,S\,O_4 + Fe_2O_3 + 2\,SO_2 \quad \text{(Eq .21)}$$

$$2\,Cu\,Fe\,S_2 \rightarrow Cu_2\,S + 2\,Fe\,S + S \quad \text{(Eq. 22)}$$

$$Fe\,S \rightarrow Fe_3O_4 \rightarrow Fe_2O_3 \quad \text{(Eq. 23)}$$

$$Cu_2\,S \rightarrow Cu_2\,O \rightarrow \;\; Cu\,S\,O_4 \rightarrow Cu\,O.Cu\,S\,O_4 \rightarrow Cu\,O \rightarrow Cu\,Fe_2O_4 \quad \text{(Eq. 24)}$$

The previous equations also concur with those presented by Prasad and Pandey [24] for FeS oxidation, in which the presence of FeS_2, Fe_3O_4 and unoxidized FeS between 375 and 425°C and Fe_2O_3 and $Fe_2(SO_4)_3$ plus unoxidized FeS at 475°C and over, was demonstrated.

TGA Stage II, corresponding to 425–570°C. In this thermal range, an increase in the crucible mass of 16 wt% for Sample 1 and 13 wt% for Sample 2 was observed.

This stage saw a net SO_2 emission. Burger [29] reported that in temperatures below 500°C the main reaction corresponds to that presented in Eq. (25), and above 500°C to that described in Eq. (26) and Eq. (27).

$$2\,Cu_2S + 5\,O_2 \rightarrow 2\,CuO + 2\,CuSO_4 \quad \text{(Eq. 25)}$$

$$Cu_2S + 2\,CuSO_4 \rightarrow 3\,SO_2 + 2\,Cu_2O \quad \text{(Eq. 26)}$$

$$Cu_2S + 4\,CuSO_4 \rightarrow 5\,SO_2 + 6\,CuO \quad \text{(Eq. 27)}$$

Meunier and Vanderpoorten [30] and Prasad and Pandey [24] confirmed the same reactions in TGA Stage I, because in temperatures above 525 °C the only compounds present were FeS, $Fe_2(SO_4)_3$ and Fe_2O_3 (the latter being the final product of oxidation). Therefore, a possible chemical reaction at these temperatures would be oxidation of FeS to $Fe_2(SO_4)_3$ and its subsequent oxidation to Fe_2O_3 (Eqs. (31) and (32)), or direct oxidation of FeS to Fe_2O_3 (Eq. (33)).

The changes in slope in higher temperatures due to the presence of kinetic barriers formed by the generated products that hinder oxygen diffusion have been explained by Niwa [31] and Schwab and Philinis [23]. They showed that the reaction rate in the temperature zone studied was almost independent of the temperature in this region, so that the kinetics, the rate of diffusion of oxygen through the pores in the ferric oxide layers produced, must be controlled. Some authors [8, 32] reported that Cu_2O is oxidized to CuO under high temperatures. Furthermore, above 400°C, oxidation of S and the continued degradation of Cu_2S occurs resulting in the formation of different Cu_xO compounds, although the most frequently reported compound within these temperatures is Cu_2O (Eqs. (28) and (29)). The following equations are proposed to explain the reactions that may have taken place in this TGA stage:

$$4\,Cu_2S + 7\,O_2 \rightarrow 2\,Cu_2O + 2\,Cu_2SO_4 + SO_2 \quad \text{(Eq. 28)}$$

$$3Cu_2S + 6\,O_2 \rightarrow 2\,Cu_2O + 2\,CuSO_4 + SO_2 \quad \text{(Eq. 29)}$$

$$3\,Cu_2O + Cu_2S + 6\,CuSO_4 + 4O_2 \rightarrow 7\,(CuO \cdot CuSO_4) \quad \text{(Eq. 30)}$$

$$2\ Fe\ S + 5\ O_2 + SO_2 \rightarrow Fe_2\ (SO_4)_3 \quad \text{(Eq. 31)}$$

$$2\ Fe_2\ (SO_4)_3 \rightarrow 2\ Fe_2O_3 + 6\ SO_2 + 3\ O_2 \quad \text{(Eq. 32)}$$

$$Fe\ S \rightarrow Fe_3O_4 \rightarrow Fe_2O_3 \quad \text{(Eq. 33)}$$

TGA Stage III, corresponding to 570–685°C. No change in weight measurements at this temperature interval was found. Data reported by Schwab and Philinis [23] and Prasad and Pandey [24] showed that, as in the previous stage studied, the rate of oxide formation did not change with temperature, attributing the non-reactivity to the closure of the pores of the material, which prevents the diffusion of oxygen into the sample.

TGA Stage IV, corresponding to 685–870°C. A very pronounced decrease in the TGA curve was observed at this stage. From 685°C upwards, a weight loss was observed reaching levels similar to those found inside the crucible in temperatures around 870°C. The loss of S in the samples can be associated to this phase. At this stage, the rate of weight loss is very high, however, once approximately 90–95 % of the weight loss has occurred (at 850-870°C), the rate decreases rapidly to zero. The weight loss found was 55 % for Mixture_1 (65 wt% Cu) and 51 % for Mixture_2 (73 wt% Cu).

The total oxidation of chalcopyrite [30] and pyrite [24] has been reported for this thermal range (685–870 °C). At 870 °C, samples that completely converted to Fe_2O_3 and CuO were found. Oxidation of copper sulfides in the 750°-950 °C range has also been documented by Ramakrishna and Abraham [33], presenting possible equations to explain the reactions that can be expected to take place in that temperature range (Eq. (34)–(37)). For the range between 685 and 870 °C, the main characteristic of the TGA curve was a negative slope related to the massive production of sulfur dioxide. The desulfurization process leads to the conversion of copper sulfate and oxysulfate into copper oxides (CuO, Cu_2O).

$$2Cu_2S\cdot + 3O_2 \rightarrow 2\ Cu_2O + SO_2 \quad \text{(Eq. 34)}$$

$$Cu_2O\cdot + \frac{1}{2}\ O_2 \rightarrow 2\ CuO \quad \text{(Eq. 35)}$$

$$Cu_2S\cdot + 2\ CuO \rightarrow 6\ Cu + SO_2 \quad \text{(Eq. 36)}$$

$$(CuO\cdot CuSO_4) \rightarrow 2\ CuO + \frac{1}{2}\ O_2 + SO_2 \quad \text{(Eq. 37)}$$

Otherwise, according to the findings of Dunn and Muzenda [27], the CuO produced due to the decomposition of sulfates is shown in Eq. (38).

$$2\ CuSO_4 \rightarrow CuO\cdot CuSO_4 + SO_3 \quad \text{(Eq. 38)}$$

The Fe_2O_3 produced remains unreacted in this stage.

TGA Stage V, corresponding to 870–1030°C. In this range, the crucible mass remains constant up to 1030°C. As the reaction advance seemed to be independent of temperature in this range, we propose that the reaction rate is controlled by the rate of oxygen diffusion through the pores of material within the crucible.

TGA Stage VI, corresponding to 1030–1200°C. In this thermal range, the deoxygenation of residual oxides produced a slight but constant weight loss estimated at around 6 % for Mixture_1 (65 wt%Cu) and 5 % for Mixture_2 (73 wt%Cu) at 1200°C. In this stage, the sulfur is totally eliminated from the crucible. In agreement with Li and Mayer [34] and Yi [35], the observed mass drop in oxygen loss in the oxides produced may be due to Eqs. (39) and (40).

$$4\ CuO \rightarrow 2\ Cu_2O + O_2 \quad \text{(Eq. 39)}$$

$$Fe_3O_4 \rightarrow Fe_2O_3 \quad \text{(Eq. 40)}$$

3.2. Activation energy evolution during thermal oxidation of the mixtures

This study evaluated the kinetic methods of Friedman, Coats, Kissinger and Flynn, and the results for each model are shown in Table 4.

The method proposed by Kissinger-Akahira-Sunose to explain (as a whole) the oxidation evolution of Cu_2S–FeS mixtures seems be the most appropriate, as demonstrated by the higher R^2 value. Studies by Sánchez-Jiménez [36] and Vyazovkin [11] demonstrated the good applicability of this method in different nonlinear temperature programs. The effectiveness of the method in this study, which involves exothermic and endothermic reactions as well as mass gain and loss, is especially important. In addition, the values for the regression coefficients in the Coats-Redfern model (1st order) were calculated, and higher values than those obtained for Coats-Redfern (2nd order) found. As a result, due to the discovery of the higher value for the regression coefficient for the first-order modeling, the assumption that this is the dominant reaction order for almost all the reactions listed can be corroborated. Moreover, the method proposed by Friedman seems to be poorly suited to the kinetic study of Cu_2S–FeS mixtures.

The activation energy, as discussed in section 2.5 for the Kissinger-Akahira-Sunose method, from the slope of the plot of $ln\left(\frac{\beta}{T^2}\right)$ versus $\frac{1000}{T}$, can be determined (Fig. 2).

A positive upward evolution in the activation energy with respect to the conversion degree for both mixtures can be observed. The corresponding values for Mixture_1 (65 wt%Cu) are, in the overall conversion range, higher than the calculated values for Mixture_2 (73 wt%Cu). This difference in the higher value of the activation energy for FeS oxidation (120–175 kJ mol^{-1}) [37] compared to that found for Cu_2S oxidation (25–104 kJ mol^{-1}) can be attributed. Additionally, that difference increases in direct correlation to the degree of conversion in both studied mixtures. The study by Coombs and Munir [25] of FeS oxidation in the 648 to 650°C temperature range corroborates these estimates. These authors demonstrated that the oxidation kinetics of this compound in the step from $Fe_2(SO_4)_3$ to Fe_2O_3 are controlled, calculating a value of 192 kJ mol^{-1} for this activation energy. Prasad and Pandey [24] reported the apparent activation energy for FeS oxidation in the range of 192 kJ mol^{-1}. However, Niwa [31] calculated an activation energy of Ea = 21.4 kJ mol^{-1} for the reaction shown by Eq. (41).

$$Fe\ S_{1-x} + \left(\frac{7}{4} + x\right)\ O_2 \leftrightarrow \frac{1}{2}\ Fe_2\ O_3 + (1-x)\ S\ O_2 \quad \text{(Eq. 41)}$$

3.3. Oxidation reactions of Cu2S–FeS

The reactions that occur during the oxidation of a Cu_2S–FeS mixture were determined by thermodynamic calculations with a model developed for this work. The model reproduces the TGA experimental curve by calculating the chemical equilibrium for small intervals in the thermal increase during the TGA test. As the temperature increases, the material in the crucible reacts with the oxygen flowing into the TGA device. This thermodynamic approach enabled us to reproduce the reactions within the crucible and the weight evolution of the crucible as registered by the TGA curve.

Table 4
Shows the results of the application of the different methods presented in Table 3. Mixture_1 corresponds to the sample composed of 65% Cu, and Mixture_2 to the sample consisting of 73% Cu.

Method	Mixture_1		Mixture_2	
	R^2	df	R^2	df
Friedman	0.849	1.966	0.880	1.978
Coats- Redfern (1st order)	0.992	1.966	0.989	1.978
Coats- Redfern (2nd order)	0.913	1.966	0.936	1.978
Kissinger-Akahira-Sunose	0.997	1.966	0.998	1.978
Flynn - Wall -Ozawa	0.651	1.966	0.701	1.978

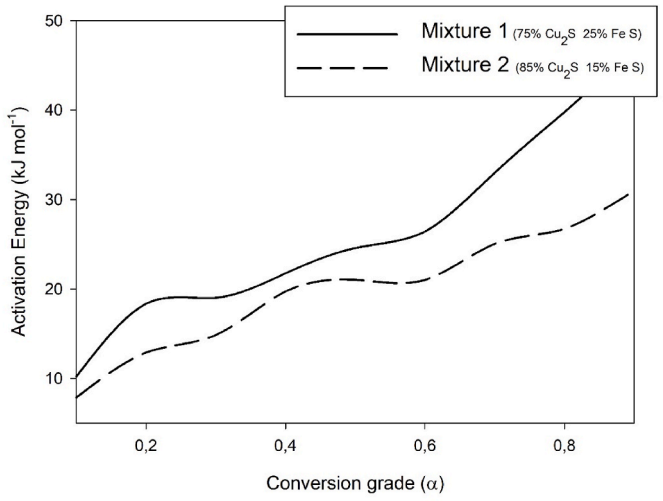

Fig. 2. Activation energy evolution calculated by the Kissinger-Akahira-Sunose method for both Cu_2S–FeS mixtures.

Real oxygen efficiency could be determined, since the oxygen availability was used as a limiting factor to calculate the progress of each reaction, and fit them to the empirically calculated TGA test data. It was possible to overlap the thermodynamically calculated mass with the real mass inside the crucible with great accuracy.

The chain of reactions produced in the TGA, as developed thermodynamically, is described in Table 5. Ten different reactions for the Cu_2S–FeS oxidation process were obtained by computational calculations.

In Fig. 3, the experimental TGA curve of the oxidation process is shown in a continuous line, and the thermodynamically calculated curve in a dotted line. On the thermodynamically calculated curve, the starting temperatures of each reaction determined by the model developed are indicated. The dashed line shows the SO_2 percentage measured during the TGA test.

Table 5
Reactions for each temperature range for Cu_2S–FeS mixtures in an oxidative environment during thermal degradation. The FactSage Equilib module was used to make the calculations.

Temperature ranges (°C)	Reactions	
300–340.3	$10\ Cu_2S + 8\ FeS + 11/2\ O_2 = Fe_2O_3 + 2\ FeSO_4 + 4\ Cu_5FeS_4$	(Eq. 42)
340.3–353.7	$4\ FeS + Fe_2O_3 + 4\ Cu_5FeS_4 + 37/2\ O_2 = 10\ Cu_2S + 10\ FeSO_4$	(Eq. 43)
353.7–424.2	$7\ Cu_2S + FeS + 16\ O_2 = FeSO_4 + 7\ Cu_2SO_4$	(Eq. 44)
424.2–456.9	$3\ Cu_2S + FeS + 107 Cu_2SO_4 + 57/2\ O_2 = 59\ Cu_2O + 101\ CuSO_4 + 1/2\ (Cu_2O)(Fe_2O_3) + 10\ SO_2$	(Eq. 45)
456.9–519.9	$3\ Cu_2S + FeS + 4Cu_2O + 5CuSO_4 + 23/2\ O_2 = 1/2\ (Cu_2O)(Fe_2O_3) + 9\ (CuO)(CuSO_4)$	(Eq. 46)
519.9–539.5	$3\ Cu_2S + FeS + 20\ Fe_2O_3 + 79/2\ (Cu_2O)(Fe_2O_3) + 59/2O_2 = 30\ Fe_3O_4 + 4\ (CuO)(CuSO_4) + 17\ CuO + CuFe_2O_4 + 28\ FeCu_2O_4 + Cu(Cu_2O_4)$	(Eq. 47)
539.5–675.1	$3\ Cu_2S + FeS + 7/2\ Fe_3O_4 + 10\ CuO + 7/2\ FeCu_2O_4 + 6\ O_2 = 15/2\ (Cu_2O)(Fe_2O_3) + 4\ (CuO)(CuSO_4)$	(Eq. 48)
675.1–787.9	$7\ (CuO)(CuSO_4) + FeCu_2O_4 = 14\ CuO + 1/2\ CuFe_2O_4 + 1/2\ Cu(CuO_4) + 7/2\ O_2 + 7SO_2$	(Eq. 49)
787.9–873.5	$7\ (CuO)(CuSO_4) = 14\ CuO + 7/2\ O_2 + 7SO_2$	(Eq. 50)
1118.5–1228.5	$CuO + SPINEL = Cu_2O + MATTE + O_2$	(Eq. 51)

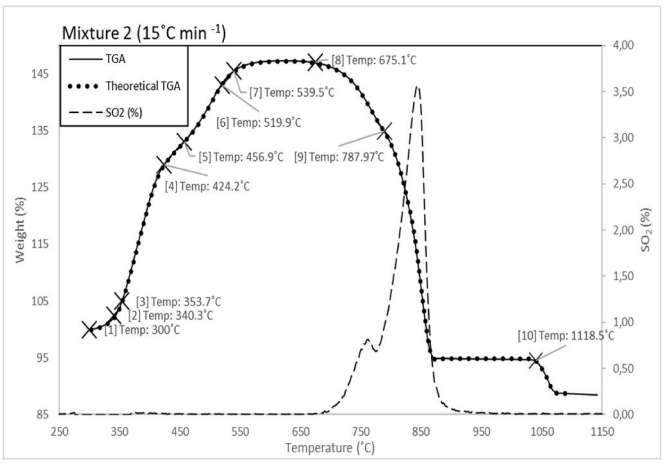

Fig. 3. Theoretical modelling of the TGA curve (mixture with 73 wt%Cu) for a heating rate of 15 °C min^{-1}. Dashed line shows the SO_2 wt% produced during the TGA test.

The initial mass variation starts at 300°C, with the increase in crucible weight due to Cu_2S and FeS oxidation (Eq. 42). The first mass increase is related to iron sulfation at between 300°C and 424.2°C (Eq. 42–44).

The reactions obtained in this study for the first mass increase up to 424.2°C match those described by Coombs and Munir [25] and Kennedy and Sturman [26] for Fe sulfation, and the initial appearance of Fe_2O_3. Asaki [38] reported that the first mass gain from Cu_2S oxidation yields Cu_5FeS_4, as in the equation described in this work (Eq. 42).

Following the initial mass increase, a different reaction occurs at 424.2°C. In this stage, the residual Cu_2S and FeS, together with the products of the previous reactions, react with oxygen to produce (Cu_2O)(Fe_2O_3), Cu_2O and $CuSO_4$, as described by Dunn and Muzeda [27], Nafees [39] and Prasad and Pandey [24] (Eq. 45).

In the 456.9-519.9°C temperature range, the residual Cu_2S and FeS, as well as Cu_2O, $CuSO_4$ produced in the previous stage, react with oxygen to produce (Cu_2O)(Fe_2O_3) and (CuO)($CuSO_4$), as described in reaction 46. These same products were described by Nafees [39], Dunn and Muzeda [27], Prasad and Pandey [24] and Burger [29].

At 519.9°C (Eq. 47), a mix of Cu_2S, FeS, Fe_2O_3 and (Cu_2O)(Fe_2O_3) produced in the last reaction stage leads, through oxidation, to the formation of Fe_3O_4, CuO and (CuO)($CuSO_4$), as well as spinels such as $CuFe_2O_4$, as determined by Asaki [38], Nafees [39], Dunn and Muzeda [27], Prasad and Pandey [24] and Burger [29].

The final mass gain stage is between 539.5 and 675.1°C. In this stage, reaction 48 takes place where the last residual Cu2S and FeS, together with the previously produced components, react to produce (Cu_2O)(Fe_2O_3) and (CuO)($CuSO_4$), as also described by Asaki [38], Nafees [39], Dunn and Muzeda [27], Prasad and Pandey [24] and Burger [29].

From 675.1°C, mass loss starts with reaction 49. At this temperature, CuO starts to form, as described by Nafees [39] and Prasad and Pandey [24]. The thermodynamic model shows that SO_2 starts to be produced at the same moment as it is registered by the DOAS device. The production of CuO and SO_2 extends to 873.5°C (Eq. 49 and 50), which corresponds to the large mass loss (TGA Stage IV of section 3.2 of this work).

The reactions described above, 49 and 50, are highly exothermic, producing a higher temperature increase around the particles within the crucible than the temperature registered by the thermocouple near the crucible. The modeled curve shifted to the right with respect to the TGA curve at this stage. In order to correct this deviation, the temperature used for the model calculations in this stage was higher than the registered TGA temperature. For this reason, the last of the reactions described (Eq. 51) might not happen at the temperature of 1040°C recorded by the TGA equipment but at 1118.5°C described by the

thermodynamic model calculations. In this last reaction (Eq. (38)), Cu_2O is oxidized to CuO, and the material inside the crucible reaches sufficient temperature to melt and produce liquid matte.

4. Conclusions

The thermal degradation process in an oxidative environment has been studied for samples of Cu_2S–FeS mixtures using TGA. The Friedman, Coats-Redfern, Kissinger-Akahira-Sunose and Flynn-Wall-Ozawa kinetic models were all evaluated and the Kissinger-Akahira-Sunose method was found to be the most suitable for the kinetic study of Cu_2S–FeS mixtures. The kinetic parameters calculated using the selected method are highly dependent on the degree of conversion, such as the activation energy ranging between 10 and 20 Kj mol^{-1} for conversion rates of 0.2, and between 30 and 50 Kj mol^{-1} for conversion rates of 0.9.

A computational model based on thermodynamics was developed to reproduce the TGA curve of the Cu_2S–FeS samples. The results obtained are high reliable, as the calculated and empirical curve fit are very close. The reactions that happened during the thermal degradation of the Cu_2S–FeS mixture in an oxidative environment between 300°C and 1228.5°C were determined, yielding 10 reactions and the identification of 13 different phases in addition to Cu_2S and FeS.

CRediT authorship contribution statement

M.Vázquez Vázquez: Conceptualization, Methodology, Investigation, Formal analysis, Writing – original draft, Writing – review & editing, Validation. **M.J. Díaz Blanco:** Conceptualization, Methodology, Investigation, Formal analysis, Writing – original draft, Writing – review & editing, Validation. **R.A. Parra Figueroa:** Conceptualization, Methodology, Investigation, Formal analysis, Writing – original draft, Writing – review & editing, Validation. **E.R. Balladares Varela:** Conceptualization, Methodology, Investigation, Formal analysis, Writing – original draft, Writing – review & editing, Validation. **O. Jerez Riveros:** Conceptualization, Methodology, Investigation, Formal analysis, Writing – original draft, Writing – review & editing, Validation. **M. Cuevas Cerda:** Conceptualization, Methodology, Investigation, Formal analysis, Writing – original draft, Writing – review & editing, Validation. **I. Moreno-Ventas Bravo:** Conceptualization, Methodology, Investigation, Formal analysis, Writing – original draft, Writing – review & editing, Validation.

Declaration of competing interest

The authors declare that they have no known competing financial interests or personal relationships that could have appeared to influence the work reported in this paper.

Data availability

The data that has been used is confidential.

Acknowledgements

This work was carried out with financial support from the Research and Transfer Policy Strategy of the University of Huelva (Call for Industrial Doctorate grants at the University of Huelva). The authors also wish to thank the GEA Institute of the Universidad de Concepción, Chile, whose facilities were made available to us to carry out a significant part of the experimental work performed.

References

[1] W.G. Davenport, M.J. King, M.E. Schlesinger, A.K. Biswas, Extractive Metallurgy of Copper, Elsevier, 2002.
[2] M. Laputka, W. Xie, A review of recent advances in pyrometallurgical process measurement and modeling, and their applications to process improvement, Min. Metal. Explorat. 38 (2021) 1135–1165, https://doi.org/10.1007/s42461-021-00386-y.
[3] P. Barrios. Cinética en la etapa de conversión para la obtención pirometalúrgico del cobre, Seville Univ., Seville, 2004. Ph.D. Thesis.
[4] T.M. Morris, History of copper converting, J. Occup. Med. 20 (7) (1968) 73–75.
[5] R.R. Moskalyk, A.M. Alfantazi, Review of copper pyrometallurgical practice: today and tomorrow, Miner. Eng. 16 (10) (2003) 893–919.
[6] U. Platt, J. Stutz. Differential Optical Absorption Spectroscopy, 2008 doi:10.1007/978-3-540-75776-4.7.
[7] A. Ulvan, M.R. Maluana, M.A. Batubara, N.A. Melvi. The Technical Concept of Differential Optical Absorption Spectroscopy for SO2 Gas Spectrum Monitoring on Volcanic, Ash of Gunung Anak Krakatau Volcano, Atlantis Press, 2021, pp. 137–143.
[8] X. Wang, Z. Huang, M. Wei, T. Lu, D. Nong, J. Zhao, L. Teng, Catalytic effect of nanosized ZnO and TiO2 on thermal degradation of poly(lactic acid) and isoconversional kinetic analysis, Thermochim. Acta 672 (2019) 14–24, https://doi.org/10.1016/j.tca.2018.12.008.
[9] S. Hasani, M. Panjepour, M. Shamanian, Non-isothermal kinetic analysis of oxidation of pure aluminum powder particles, Oxid. Metals 81 (3–4) (2013) 299–313, https://doi.org/10.1007/s11085-013-9413-z.
[10] S. Hasani, P. Rezaei-Shahreza, A. Seifoddini, The effect of Cu minor addition on the non-isothermal kinetic of nano-crystallites formation in Fe41Co7Cr15Mo14Y2C15B6 BMG, J. Therm. Anal. Calorim. 143 (5) (2020) 3365–3375, https://doi.org/10.1007/s10973-020-09716-6.
[11] S. Vyazovkin, A.K. Burnham, J.M. Criado, L.A. Pérez-Maqueda, C. Popescu, N. Sbirrazzuoli, ICTAC Kinetics Committee recommendations for performing kinetic computations on thermal analysis data, Thermochim. Acta 520 (2011) 1–19, https://doi.org/10.1016/j.tca.2011.03.034.
[12] J. Yang, S. Liu, Q. Dai, Z. Guo, R. Ao, J. Pan, L. Ma, Regeneration mechanism of CuO-CaSO4 based oxygen carriers, Fuel 306 (2021), 121668, https://doi.org/10.1016/j.fuel.2021.121668.
[13] H.L. Friedman, Kinetics of thermal degradation of char-forming plastics from thermogravimetry. Application to a phenolic plastic, J. Polym. Sci. Part C: Polymer Symposia 6 (1) (1964) 183–195, https://doi.org/10.1002/polc.5070060121.
[14] A.W. Coats, J.P. Redfern, Kinetic parameters from thermogravimetric data, Nature 201 (4914) (1964) 68–69, https://doi.org/10.1038/201068a0.
[15] H.E. Kissinger, Reaction kinetics in differential thermal analysis, Anal. Chem. 29 (11) (1957) 1702–1706, https://doi.org/10.1021/ac60131a045.
[16] T. Ozawa, A modified method for kinetic analysis of thermoanalytical data, J. Therm. Anal. 9 (3) (1976) 369–373, https://doi.org/10.1007/bf01909401.
[17] R. Ebrahimi-Kahrizsangi, M. Abbasi, Evaluation of reliability of Coats-Redfern method for kinetic analysis of non-isothermal TGA, Trans. Nonferrous Metals Soc. China 18 (1) (2008) 217–221, https://doi.org/10.1016/s1003-6326(08)60039-4.
[18] J.H. Flynn, L.A. Wall, General treatment of the thermogravimetry of polymers, J. Res. National Bureau Standards Section A: Phys. Chem. 70A (6) (1966) 487, https://doi.org/10.6028/jres.070a.043.
[19] C.W. Bale, P. Chartrand, S.A. Degterov, G. Eriksson, K. Hack, Mahfoud, S. Petersen, FactSage thermochemical software and databases, Calphad 26 (2) (2002) 189–228.
[20] C.W. Bale, E. Bélisle, P. Chartrand, S.A. Decterov, G. Eriksson, Hack, S. Petersen, FactSage thermochemical software and databases—recent developments, Calphad 33 (2) (2009) 295–311.
[21] C.W. Bale, E. Bélisle, P. Chartrand, S. Decterov, G. Eriksson, A. Gheribi, K. Hack, I. H. Jung, Y.B. Kang, J. Melançon, FactSage thermochemical software and databases 2010–2016, Calphad 35–53 (2016).
[22] Montreal FactSage, Canada. Available online: www.factsage.com. (Accessed 16 April 2023).
[23] G.M. Schwab, J. Philinis, Reactions of iron pyrite: its thermal decomposition, reduction by hydrogen and air oxidation, J. Am. Chem. Soc. 69 (1974) 2588–2596, 1947.
[24] S. Prasad, B.D. Pandey, Alternative processes for treatment of chalcopyrite-a review, Miner. Eng. 11 (8) (1998) 763–781, https://doi.org/10.1016/S0892-6875(98)00061-2.
[25] P.G. Coombs, Z.A. Munir, The mechanism of oxidation of ferrous sulfide (FeS) powders in the range of 648 to 650 °C, Metall. Mater. Trans. B 20 (1989) 661–670, https://doi.org/10.1007/BF02655922.
[26] T. Kennedy, B.T. Sturman, The oxidation of iron(II) sulphides, J. Therm. Anal. Calorim. 8 (2) (1975) 329–337, https://doi.org/10.1007/BF01904010.
[27] J.G. Dunn, C. Muzenda, Quantitative analysis of phases formed during the oxidation of covellite (CuS), J. Therm. Anal. Calorim. 64 (3) (2001) 1241–1246, https://doi.org/10.1023/A:1011513616930.
[28] Z. Asaki, Y. Kondo, Oxidation kinetics of iron sulfide in the form of dense plate, pellet and single particle, J. Therm. Anal. 35 (1989) 1751–1759, https://doi.org/10.1007/BF01911664.
[29] E. Burger, D. Bourgarit, V. Frotté, F. Pilon, Kinetics of iron–copper sulphides oxidation in relation to protohistoric copper smelting, J. Therm. Anal. Calorim. 103 (1) (2011) 249–256.
[30] L. Meunier, H. Vanderpoorten, Roasting reactions of chalcopyrite, ATB Met 1 (1957) 31–35.
[31] K. Niwa, T. Wada, Y. Shiraishi, Roasting reaction of ferrous sulfide, J. Occup. Med. 9 (1957) 269–273, https://doi.org/10.1007/BF03398487.
[32] Y. Zuo, Y. Liu, J. Li, R. Du, X. Han, T. Zhang, j. Arbiol, N.J. Divins, J. Llorca, N. Guijarro, K. Sivula, A. Cabot, In situ electrochemical oxidation of Cu2S into CuO nanowires as a durable and efficient electrocatalyst for oxygen evolution reaction, Chem. Mater. 31 (18) (2019) 7732–7743, https://doi.org/10.1021/acs.chemmater.9b02790.

[33] V. Ramakrishna Rao, K.P. Abraham, Kinetics of oxidation of copper sulfide, Metall. Trans. A 2 (9) (1971) 2463–2470.
[34] J. Li, J. Mayer, Oxidation and reduction of copper oxide thin films, Mater. Chem. Phys. 32 (1) (1992) 1–24, https://doi.org/10.1016/0254-0584(92)90243-2.
[35] F. Yi, J.B. DeLisio, N. Nguyen, M.R. Zachariah, D.A. LaVan, High heating rate decomposition dynamics of copper oxide by nanocalorimetry-coupled time-of-flight mass spectrometry, Chem. Phys. Lett. 689 (2017) 26–29, https://doi.org/10.1016/j.cplett.2017.09.066.
[36] P. Sánchez-Jiménez, J. Criado, L. Pérez-Maqueda, Kissinger kinetic analysis of data obtained under different heating schedules, J. Therm. Anal. Calorim. 94 (2) (2008) 427–432, https://doi.org/10.1007/s10973-008-9200-2.
[37] J.M. Lambert, G. Simkovich, P.L. Walker, The kinetics and mechanism of the pyrite-to-pyrrhotite transformation, Metall. Mater. Trans. B 29 (2) (1998) 385–396, https://doi.org/10.1007/s11663-998-0115-x.
[38] Z. Asaki, S. Ando, Y. Kondo, Oxidation of molten copper matte, Metall. Trans. A B 19 (1) (1988) 47–52.
[39] M. Nafees, M. Ikram, S. Ali, Thermal behavior and decomposition of copper sulfide nanomaterial synthesized by aqueous sol method, Dig. J. Nanomater. Biostruct. 10 (2) (2015) 635–641.